



HAL
open science

STA-based design of an adaptive disturbance observer for autonomous underwater vehicles: From concept to real-time validation

Jesús Guerrero, Ahmed Chemori, Jorge Torres, Vincent Creuze

► To cite this version:

Jesús Guerrero, Ahmed Chemori, Jorge Torres, Vincent Creuze. STA-based design of an adaptive disturbance observer for autonomous underwater vehicles: From concept to real-time validation. *Control Engineering Practice*, 2024, 144, pp.105831. 10.1016/j.conengprac.2023.105831 . lirmm-04364453

HAL Id: lirmm-04364453

<https://hal-lirmm.ccsd.cnrs.fr/lirmm-04364453v1>

Submitted on 27 Dec 2023

HAL is a multi-disciplinary open access archive for the deposit and dissemination of scientific research documents, whether they are published or not. The documents may come from teaching and research institutions in France or abroad, or from public or private research centers.

L'archive ouverte pluridisciplinaire **HAL**, est destinée au dépôt et à la diffusion de documents scientifiques de niveau recherche, publiés ou non, émanant des établissements d'enseignement et de recherche français ou étrangers, des laboratoires publics ou privés.

Highlights

STA-based design of an adaptive disturbance observer for autonomous underwater vehicles: from concept to real-time validation

Jesús Guerrero,Ahmed Chemori,Vincent Creuze,Jorge Torres

- A new adaptive disturbance observer is proposed for unnamed underwater vehicles.
- The stability analysis of the resulting closed-loop controller/observer is provided.
- Real-time experiments demonstrate the effectiveness and robustness of the proposed solution.

STA-based design of an adaptive disturbance observer for autonomous underwater vehicles: from concept to real-time validation

Jesús Guerrero^a, Ahmed Chemori^{b,*}, Vincent Creuze^b and Jorge Torres^c

^a*Mechatronics Department, Tecnológico Nacional de México / ITS Abasolo, Guanajuato, México*

^b*LIRMM, University of Montpellier, CNRS, Montpellier, France*

^c*Center for Research and Advanced Studies of the National Polytechnic Institute (CINVESTAV), México city, México*

ARTICLE INFO

Keywords:

Disturbance Observer
Super-Twisting Algorithm
AUV
Stability Analysis
Real-Time experiments

ABSTRACT

In this paper, we propose to improve the robustness of the well-known PD controller through an adaptive disturbance observer. The proposed disturbance observer is based on the Super-Twisting Algorithm, and is designed with adaptive gains. The stability analysis of the resulting closed-loop controller/observer is achieved using Lyapunov arguments. Real-time experiments in different operating conditions are conducted to demonstrate the effectiveness as well as robustness of the proposed methodology, compared to the nominal PD controller.

1. Introduction and Related Work

The current trend in trajectory tracking control of AUVs is focused on searching for advanced control schemes to deal with the multiple challenges of their nonlinear dynamics, with unknown, time-varying and thereby difficult-to-estimate parameters, in addition to operating in the presence of unpredictable random disturbances. Examples of such approaches include Fuzzy Logic Controllers (FLC) Xiang, Yu, Lapiere, Z. and Z. (2015), Khodayari and Balochian (2015), Neural-Network based control (NNC) Cui, Chen, Yang and Chen (2017); Yan, Wang and Xu (2019), Model Predictive control Shen, Shi and Buckham (2018), Adaptive control Li and Lee (2005), Sliding Mode Control (SMC) García-Valdovinos, Salgado-Jiménez, Bandala-Sánchez, Nava-Balazar, Hernández-Alvarado and Cruz-Ledesma (2014), High Order Sliding Modes Control (HOSMC) Ismail and Putranti (2015); Guerrero, Torres, Antonio and Campos (2018), and deep learning based control Li, Wang and Ma (2022). Each methodology from the literature has mainly both strengths and weaknesses. For instance, FLC has a simple structure, making its design easy and cost-effective. However, this controller's tuning might be difficult, because it has no stability criterion to guide this process.


On the other hand, one may ascertain the constant interest in reinforcing the prominent place PD controllers have gained in several applications. The goal is to take advantage of the classic PD/PID controllers (including acceptable performance, ease of design, cost, etc.) to face the challenges of complex nonlinear dynamics of robotic systems like AUVs. To this end, PD/PID controllers have


been improved by adopting several strategies based on auto-tuning Zhang, Zhang, Liu, Zhou and Papavassiliou (2018), saturation Sarhadi, Noei and Khosravi (2016a), adaptation Khodayari and Balochian (2015), MR adaptive PID Sarhadi, Ranjbar and Khosravi (2016b) or nonlinear time-varying functions Campos, Chemori, Creuze, Torres and Lozano (2017); Guerrero, Torres, Creuze and Chemori (2019a). For instance, a nonlinear PID for the trajectory tracking of an AUV has been proposed in Guerrero, Torres, Creuze, Chemori and Campos (2019b).

In general, the above-mentioned approaches present good performance in the presence of unmodeled parametric uncertainties and dynamic disturbances; however, it can be seriously degraded by ubiquitous exogenous disturbances often present in marine environments Tijjani, Chemori and Creuze (2022). Nonlinear observers may constitute a potential candidate to estimate unknown external perturbations of an AUV, and can be easily integrated in any control scheme. The stability of the resulting controller-observer structure in closed loop is not simple to prove theoretically; where it is essential to reject the external disturbance asymptotically or in finite time. Disturbance observers include those based on sliding modes Hall and Shtessel (2006), high-gain observers Fernandes, Sørensen, Pettersen and Donha (2015), and the Extended State Observers (ESO) Guo, Zhang, Celler and Su (2016). Second-order sliding mode observers are prioritized in this work since they provide robustness along with chattering attenuation and continuous estimation. This is an improvement w.r.t. the basic sliding mode algorithm, as demonstrated by Levant (1993).

In practice, introducing nonlinear saturation functions to replace the constant feedback gains of standard Proportional-Derivative (PD) or Proportional-Integral-Derivative (PID) control strategies can improve their performance and robustness. This has led to the development of a family of nonlinear control strategies so-called NLPD (Nonlinear PD) and NLPID (NonLinear PID), Campos et al. (2017), Guerrero et al. (2019b). Subsequently, in Guerrero et al. (2019a), introducing a disturbance observer based on generalized

*Corresponding author

 jesus.gt@abasolo.tecnm.mx (J. Guerrero); Ahmed.Chemori@lirmm.fr (A. Chemori); vincent.creuze@lirmm.fr (V. Creuze); jtorres@ctrl.cinvestav.mx (J. Torres)

 <https://jguerrero.github.io/> (J. Guerrero)

ORCID(s): 0000-0002-5873-8986 (J. Guerrero); 0000-0001-9739-9473 (A. Chemori)

STA (GSTA) has proven to be effective in strengthening the NLPID controller, especially in its ability to reject exogenous disturbances, which is a known weakness of the conventional NLPID algorithm alone, Guerrero et al. (2019b). This approach has been developed in several studies from the literature, and has shown promising results in practical control applications, Guerrero et al. (2019a).

The present manuscript focuses on analyzing and designing an NLPD controller enhanced with an STA-based disturbance observer to achieve reliable performance and robustness in presence of internal and external parametric disturbances. The main objective of this control approach is to maintain tracking performance while effectively rejecting external disturbances. A significant advantage of PD control over its PID counterpart is that PD control does not suffer from wind-up phenomenon when the control input is saturated, Sarhadi, Ranjbar and Khosravi (2017). From a design point of view, the simplicity of basic PD controllers is maintained, where the STA observer requires the tuning of only two parameters. Finally, the complete closed-loop stability analysis and design of the proposed control scheme are provided, which are expected to offer competitive performance and robustness compared to other control strategies. The rest of the paper is organized as follows: The mathematical modeling of underwater vehicles is given in Section 2. The design of the proposed adaptive disturbance observer, based on the Super Twisting Algorithm, is detailed in Section 3, while the stability analysis of the proposed observer is addressed in Section 4. Section 5 is devoted to the stability analysis of the nominal PD controller augmented with the proposed adaptive disturbance observer. Finally, the obtained experimental results are introduced and observed in Section 6; where several real-time experiments are conducted on a real platform. Finally, some concluding remarks are drawn in Section 7.

2. Mathematical Model of the Underwater Vehicle

The mathematical model of underwater vehicles has been studied in several works from the literature Fossen (1999, 2011); Wadoo and Kachroo (2017). To this end, reference frames are selected as illustrated in Figure 1. The dynamic model in the body-fixed frame is given as follows:

$$M\dot{v} + C(v)v + D(v)v + g(\eta) = \tau + w_v(t) \quad (1)$$

The vector $v \in \mathbb{R}^6$ is the state vector of velocity in the body-fixed frame. The inertia matrix is denoted by $M \in \mathbb{R}^{6 \times 6}$, $C(v) \in \mathbb{R}^{6 \times 6}$ is the Coriolis-centripetal matrix, $D(v) \in \mathbb{R}^{6 \times 6}$ is the hydrodynamic damping matrix, and $g(\cdot) \in \mathbb{R}^6$ is the vector of the gravitational and buoyancy forces and moments. The vector $\tau \in \mathbb{R}^6$ is the control input acting on the vehicle, and $w_v(t) \in \mathbb{R}^6$ is the vector of the external disturbances effects.

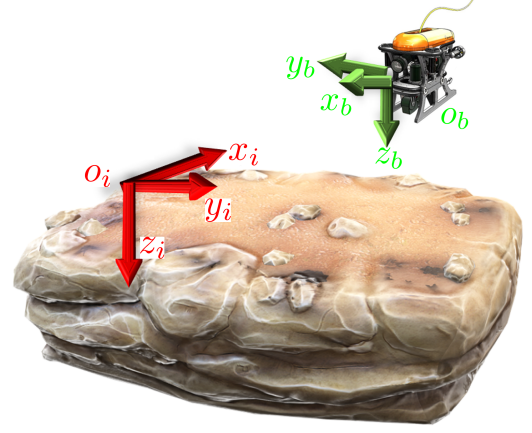


Figure 1: Illustration of the Earth-fixed frame (x_i, y_i, z_i) and the body-fixed frame (x_b, y_b, z_b) of an underwater vehicle.

The above dynamics of the underwater vehicle can be expressed in the Earth-fixed frame using the transformation matrix $J(\eta) \in \mathbb{R}^{6 \times 6}$ as follows:

$$\dot{\eta} = J(\eta)v \quad (2)$$

Where $\eta = [x, y, z, \phi, \theta, \psi]^T$ is the vector of position and orientation of the vehicle in the Earth-fixed frame, and $\dot{\eta}$ denotes its time derivative. Replacing (2) into (1) leads to the following representation in the Earth-fixed frame:

$$M_\eta(\eta)\dot{\eta} + C_\eta(v, \eta)\dot{\eta} + D_\eta(v, \eta)\dot{\eta} + g_\eta(\eta) = \tau_\eta(\eta) + \bar{w}_\eta(t) \quad (3)$$

where the different matrices are defined as follows:

$$\begin{aligned} M_\eta(\eta) &= J^{-T}(\eta)M J^{-1}(\eta) \\ C_\eta(v, \eta) &= J^{-T}(\eta) [C(v) - M J^{-1}(\eta)\dot{J}(\eta)] J^{-1}(\eta) \\ D_\eta(v, \eta) &= J^{-T}(\eta)D(v)J^{-1}(\eta) \\ g_\eta(\eta) &= J^{-T}(\eta)g(\eta) \\ \tau_\eta(\eta) &= J^{-T}(\eta)\tau \\ \bar{w}_\eta(t) &= J^{-T}(\eta)w_v(t) \end{aligned}$$

It is well known that model-based controllers require the full knowledge of the dynamical model of the vehicle. However, in underwater robotics, it is difficult to evaluate the hydrodynamic parameters because their values may depend on the operating conditions. For these reasons, we express the dynamics of the vehicle given in (3) in terms of the estimated parameters as follows:

$$\hat{M}_\eta(\eta)\dot{\eta} + \hat{C}_\eta(v, \eta)\dot{\eta} + \hat{D}_\eta(v, \eta)\dot{\eta} + \hat{g}_\eta(\eta) = \tau_\eta(\eta) + w_\eta(t) \quad (4)$$

where \hat{M}_η , \hat{C}_η , \hat{D}_η , and \hat{g}_η represent the estimation of the matrices of the dynamic model. The vector of the external disturbances $w_\eta(t)$ can be defined as:

$$w_\eta(t) = \bar{w}_\eta - \tilde{f}(\cdot) \quad (5)$$

It is worth noting that the vector $w_\eta(t)$ includes the external disturbances and the unknown dynamics of the model

denoted by $\tilde{f}(\cdot)$ and defined as:

$$\tilde{f}(\cdot) = (M_\eta - \hat{M}_\eta)\dot{\eta} + (C - \hat{C}_\eta)\dot{\eta} + (D - \hat{D}_\eta)\dot{\eta} + (g_\eta - \hat{g}_\eta) \quad (6)$$

Note that the dynamics is rewritten in terms of the known hydrodynamic parameters $\hat{f}(\cdot)$ and the lumped vector $w_\eta(t)$, including the unknown dynamics and the bounded external disturbances.

3. Proposed adaptive disturbance observer

In this section, a robust STA-Based disturbance observer is designed. The proposed methodology is based on the Extended State Observer methodology (ESO) Han (1995, 1998). In brief, the ESO technique is applied to a chain form, where the external disturbance is seen as an augmented state. Then, the ESO will be designed to estimate both the state variables and the external disturbances.

To give a comprehensive explanation of the disturbance observer, let us rewrite the dynamical model (4) in integrator chain form by considering the following state variables:

$$z_1 = \eta \quad ; \quad z_2 = \dot{\eta}$$

Then, the dynamical model (4) can be expressed as follows:

$$\begin{aligned} \dot{z}_1 &= z_2 \\ \dot{z}_2 &= \hat{F}(z) + \hat{G}(z)u(t) + d(t) \end{aligned} \quad (7)$$

Where:

$$\begin{aligned} \hat{F}(z) &= -\hat{M}_\eta(\eta)^{-1} [\hat{C}_\eta(v, \eta)\dot{\eta} + \hat{D}_\eta(v, \eta)\dot{\eta} + \hat{g}_\eta(\eta)] \\ \hat{G}(z) &= \hat{M}_\eta(\eta)^{-1} J^{-T}(\eta) \\ d(t) &= \hat{M}_\eta(\eta)^{-1} w_\eta(t) \\ u(t) &= \tau_\eta \end{aligned}$$

Finally, classical assumptions in underwater vehicles can be considered:

Assumption 1. The pitch angle is smaller than $\pi/2$, i.e., $|\theta| < \pi/2$.

Assumption 1 ensures that the inverse of the matrix $J(\eta)$ always exists; consequently, the term $G(z)$ exists. In a practical situation, a pitch close to $\pi/2$ implies that the robot dives vertically, which is mainly not required during sea missions.

Now, let us consider the following auxiliary variable defined as:

$$\sigma(t) = z_2 + \Gamma z_1 \quad (8)$$

where $\sigma \in \mathbb{R}^6$ and $\Gamma = \text{diag}\{\gamma_1, \gamma_2, \dots, \gamma_6\}$ is a diagonal positive definite matrix.

The time derivative of $\sigma(t)$ can be expressed as follows:

$$\dot{\sigma}(t) = f(z) + g(z)u(t) + d(t) \quad (9)$$

where $f(z) = \hat{F}(z) + \Gamma \dot{z}_1$, and $g(z) = \hat{G}(z)$

From the dynamics (9) of the auxiliary variable, the lumped disturbance can be considered as an extended state $h(t)$, such that:

$$\begin{aligned} \dot{\sigma}(t) &= f(z) + g(z)\tau_\eta + h(t) \\ \dot{h}(t) &= \xi(t) \end{aligned} \quad (10)$$

where $\xi(t)$ is the time derivative of the total disturbance $d(t)$.

The proposed disturbance observer dynamics for the system (10) can then be defined as:

$$\begin{aligned} \dot{\hat{\sigma}} &= f(z) + g(z)\tau_\eta - K_1 \Phi_1(\tilde{\sigma}) + \hat{d}(t) \\ \dot{\hat{d}} &= -K_2 \Phi_2(\tilde{\sigma}) \end{aligned} \quad (11)$$

Where $K_1 = \text{diag}\{k_{11}, \dots, k_{16}\}$ and $K_2 = \text{diag}\{k_{21}, \dots, k_{26}\}$ are diagonal positive definite matrices representing the observer feedback gains. The vectors Φ_1 and Φ_2 are defined as $\Phi_1(\tilde{\sigma}) = [\phi_{11}, \phi_{12}, \dots, \phi_{16}]^T$ and $\Phi_2(\tilde{\sigma}) = [\phi_{21}, \phi_{22}, \dots, \phi_{26}]^T$, where each element of these vectors is given by:

$$\phi_{1i}(\tilde{\sigma}_i) = |\tilde{\sigma}_i|^{1/2} \text{sgn}(\tilde{\sigma}_i) \quad (12)$$

$$\phi_{2i}(\tilde{\sigma}_i) = \frac{1}{2} \text{sgn}(\tilde{\sigma}_i) \quad (13)$$

for $i = \overline{1, 6}$.

Finally, the estimation errors are deduced as follows:

$$\tilde{\sigma}(t) = \hat{\sigma}(t) - \sigma(t) \quad (14)$$

$$\tilde{d}(t) = \hat{d}(t) - d(t) \quad (15)$$

where $\hat{\sigma}(t)$ and $\hat{d}(t)$ are the estimated observer internal states, $\hat{\sigma}(t)$ and $\hat{d}(t)$ represent the dynamics of the estimated observer internal states.

4. Observer Stability Analysis

Theorem 1. Consider the augmented system dynamics (10). The Super Twisting-based Algorithm (11) is a finite-time disturbance observer with the adaptive gains defined as follows:

$$k_{1i} = \omega_{1i} \sqrt{\frac{\zeta_{1i}}{2}} \quad (16)$$

$$k_{2i} = \epsilon k_{1i} \quad (17)$$

with $i = \overline{1, 6}$ and the design parameters selected as $\omega_{1i}, \zeta_{1i} > 0$.

PROOF. First of all, let us compute the time derivative of the estimation errors (14) and (15), leading to:

$$\begin{aligned} \dot{\tilde{\sigma}} &= -K_1 |\tilde{\sigma}|^{1/2} \text{sgn}(\tilde{\sigma}) + \tilde{d} \\ \dot{\tilde{d}} &= -K_2 \text{sgn}(\tilde{\sigma}) - h(t) \end{aligned} \quad (18)$$

To give a more comprehensive explanation of the stability of the proposed observer, let us consider the following change of variables:

$$s_{1i} = \tilde{\sigma}_i$$

$$s_{2i} = \tilde{d}$$

Then (18) can be rewritten in a scalar form (for $i = \overline{1,6}$) as follows:

$$\begin{aligned} \dot{s}_{1i} &= -k_{1i}|s_{1i}|^{\frac{1}{2}}\text{sgn}(s_{1i}) + s_{2i} \\ \dot{s}_{2i} &= -k_{2i}\text{sgn}(s_{1i}) + h_i(t) \end{aligned} \quad (19)$$

Without loss of generality, (19) can be rewritten, by adopting simplified notations as follows:

$$\begin{aligned} \dot{s}_1 &= -k_1|s_1|^{\frac{1}{2}}\text{sgn}(s_1) + s_2 \\ \dot{s}_2 &= -k_2\text{sgn}(s_1) + h(t) \end{aligned} \quad (20)$$

Note that if we select the state vector $\zeta = [\zeta_1, \zeta_2]^T = [|s_1|^{\frac{1}{2}}\text{sgn}(s_1), s_2]^T$, then the dynamics of ζ can be expressed as follows:

$$\dot{\zeta} = \frac{1}{2|\zeta_1|} \left\{ \begin{bmatrix} -k_1 & 1 \\ -2k_2 & 0 \end{bmatrix} \zeta + \begin{bmatrix} 0 \\ 2|\zeta_1| \end{bmatrix} h(t) \right\} \quad (21)$$

Where the following identities are always satisfied:

$$\begin{aligned} |\zeta_1| &= |s_1|^{\frac{1}{2}} \\ \text{sgn}(\zeta_1) &= \text{sgn}(s_1) \end{aligned}$$

Then, considering that the perturbation $h(t)$ is bounded, it is easy to observe that:

$$h(t) = \frac{\rho(t)}{2}\text{sgn}(\sigma) = \frac{\rho(t)}{2} \frac{\zeta_1}{|\zeta_1|} \quad (22)$$

Where $\rho(t)$ is a bounded function satisfying:

$$0 < \rho(t) < \delta_1, \quad \delta_1 > 0$$

Finally, the dynamics (20), can be rewritten as follows:

$$\dot{\zeta} = A\zeta \quad (23)$$

Where:

$$A = \frac{1}{2|\zeta_1|} \begin{bmatrix} -k_1 & 1 \\ -(2k_2 - \rho(t)) & 0 \end{bmatrix} \quad (24)$$

Now, to analyze the stability of the resulting dynamic system (21), let us consider the following Lyapunov function candidate:

$$V(\zeta, k_1, k_2) = V_0(\cdot) + \frac{1}{2\zeta_1}(k_1 - k_1^*)^2 + \frac{1}{2\zeta_2}(k_2 - k_2^*)^2 \quad (25)$$

where $\zeta_1, \zeta_2, k_1^*, k_2^*$ are positive constants and $V_0(\cdot)$ is defined as:

$$V_0(\zeta) = \zeta^T P \zeta \quad (26)$$

with:

$$P = P^T = \begin{bmatrix} \beta + 4\epsilon^2 & -2\epsilon \\ -2\epsilon & 1 \end{bmatrix} > 0 \quad (27)$$

Where β and ϵ are defined as arbitrary positive constants, then P is a positive definite matrix. Besides, note that $V_0(\cdot)$ satisfies the following inequalities:

$$\lambda_{\min}(P)\|\zeta\|_2^2 \leq V_0(\cdot) \leq \lambda_{\max}(P)\|\zeta\|_2^2 \quad (28)$$

where $\lambda_{\min}(P)$ and $\lambda_{\max}(P)$ are the smallest and greatest eigenvalues of P , respectively. The term $\|\zeta\|_2^2 = |s_1| + s_2^2$ is the Euclidean norm of ζ satisfying the inequality:

$$|\zeta_1| \leq \|\zeta\|_2 \leq \frac{V_0^{\frac{1}{2}}(\zeta)}{\lambda_{\min}^{\frac{1}{2}}(P)} \quad (29)$$

Finally, it is worth to note that the proposed Lyapunov function $V(\cdot)$ is a continuous, positive definite, and differentiable.

To compute the time derivative of $V(\cdot)$, we divide the procedure into two main steps. First, we obtain the time derivative of $V_0(\cdot)$. Second, the total time derivative of $V(\cdot)$ is found.

Step 1. Computing the time derivative of V_0 .

Consider the dynamics of ζ in (23), then, the time derivative of V_0 is computed as follows:

$$\begin{aligned} \dot{V}_0 &= 2\zeta^T P \dot{\zeta} \\ &= 2\zeta^T P A \zeta \\ &= \zeta^T (A^T P + P A) \zeta \\ &= -\frac{1}{2|\zeta_1|} \zeta^T Q \zeta \end{aligned} \quad (30)$$

where

$$Q = \begin{bmatrix} 2k_1\beta + 8\epsilon(\epsilon k_1 - k_2) + 4\epsilon\rho(t) & \star \\ 2(k_2 - \epsilon k_1) - \beta - 4\epsilon^2 - \rho(t) & 4\epsilon \end{bmatrix} \quad (31)$$

and $\star = 2(k_2 - \epsilon k_1) - \beta - 4\epsilon^2 - \rho(t)$.

Note that the matrix Q is positive definite if the gain k_2 is selected as follows:

$$k_2 = \epsilon k_1 \quad (32)$$

with a minimum eigenvalue $\lambda_{\min}(Q) \geq 2\epsilon$ if

$$k_1 > \delta_0 + \frac{\alpha_2^2}{4\epsilon\beta} + \frac{\epsilon \left[2(\beta + 4\epsilon^2 + L) + 1 \right]}{2\beta} \quad (33)$$

Finally, using (29), the time derivative of $V_0(\cdot)$ can be bounded as follows:

$$\dot{V}_0 \leq -\gamma V_0^{\frac{1}{2}}(\zeta) \quad (34)$$

with $\gamma = \mu_1 \frac{\epsilon \lambda_{\min}^{\frac{1}{2}}(P)}{\lambda_{\max}(P)}$.

Step 2. Computing the time derivative of V .

The time derivative of the Lyapunov function (25) can be expressed as follows:

$$\dot{V} = \dot{V}_0(\cdot) + \frac{1}{\zeta_1}(k_1 - k_1^*)\dot{k}_1 + \frac{1}{\zeta_2}(k_2 - k_2^*)\dot{k}_2$$

$$\begin{aligned}
 &\leq -\gamma V_0^{\frac{1}{2}}(s, k) + \frac{1}{\zeta_1}(k_1 - k_1^*)\dot{k}_1 + \frac{1}{\zeta_2}(k_2 - k_2^*)\dot{k}_2 \\
 &= -\gamma V_0^{\frac{1}{2}}(s, k) - \frac{\omega_1}{\sqrt{2\zeta_1}}|k_1 - k_1^*| - \frac{\omega_2}{\sqrt{2\zeta_2}}|k_2 - k_2^*| + \\
 &\frac{1}{\zeta_1}(k_1 - k_1^*)\dot{k}_1 + \frac{1}{\zeta_2}(k_2 - k_2^*)\dot{k}_2 + \frac{\omega_1}{\sqrt{2\zeta_1}}|k_1 - k_1^*| + \\
 &+ \frac{\omega_2}{\sqrt{2\zeta_2}}|k_2 - k_2^*| \quad (35)
 \end{aligned}$$

Using the Cauchy-Schwarz inequality, the first three terms of \dot{V} can be rewritten as:

$$-\gamma V_0^{\frac{1}{2}}(s, k) - \frac{\omega_1}{\sqrt{2\zeta_1}}|k_1 - k_1^*| - \frac{\omega_2}{\sqrt{2\zeta_2}}|k_2 - k_2^*| \leq -\pi\sqrt{V} \quad (36)$$

where $\pi = \min\{\gamma, \omega_1, \omega_2\}$.

Assuming that there exist positive constants k_1^* and k_2^* , such that $k_1 - k_1^* < 0$ and $k_2 - k_2^* < 0 \forall t \geq 0$. Then, the time derivative of V can be rewritten as follows:

$$\begin{aligned}
 \dot{V} &\leq -\pi\sqrt{V(s, k_1, k_2)} - |k_1 - k_1^*| \left(\frac{1}{\zeta_1}\dot{k}_1 - \frac{\omega_1}{\sqrt{2\zeta_1}} \right) \\
 &- |k_2 - k_2^*| \left(\frac{1}{\zeta_2}\dot{k}_2 - \frac{\omega_2}{\sqrt{2\zeta_2}} \right) \\
 &= -\pi\sqrt{V(s, k_1, k_2)} + \vartheta \quad (37)
 \end{aligned}$$

Where:

$$\begin{aligned}
 \vartheta &= -|k_1 - k_1^*| \left(\frac{1}{\zeta_1}\dot{k}_1 - \frac{\omega_1}{\sqrt{2\zeta_1}} \right) - \\
 &|k_2 - k_2^*| \left(\frac{1}{\zeta_2}\dot{k}_2 - \frac{\omega_2}{\sqrt{2\zeta_2}} \right) \quad (38)
 \end{aligned}$$

In order to preserve the finite-time convergence, it is necessary to ensure the condition $\vartheta = 0$, which can be achieved through the following adaption laws:

$$\dot{k}_1 = \omega_1 \sqrt{\frac{\zeta_1}{2}} \quad (39)$$

$$\dot{k}_2 = \omega_2 \sqrt{\frac{\zeta_2}{2}} \quad (40)$$

Roughly speaking, the adaptive gains k_1 and k_2 will be increased based on the dynamic and algebraic equations stated in (16) until the condition (33) is reached. Then, the matrix Q will be positive definite, and the finite-time convergence will be assured according to (37). Finally, when the sliding variable σ and its derivative converge to zero, the adaptive gains k_1 and k_2 will stop increasing by making $\dot{k}_1 = 0$ as $\sigma = 0$. Subsequently, the gain-adaptation law (16) is obtained.

5. Improving non-robust controllers

PD feedback control is a widely used control strategy in the field of AUVs. PD controllers are relatively simple and easy to implement, while assuming acceptable performance in controlling the vehicle's motion. Although this control scheme performs well under nominal conditions, its performance may significantly degrade when the hydrodynamic parameters of the vehicle change. To address this issue, we propose an enhanced PD controller that utilizes the ESO technique as well as an adaptive disturbance observer to estimate and compensate for external disturbances and parametric uncertainties.

First of all, let us consider the PD nominal design reported in Campos et al. (2017), and defined as:

$$\tau_{nom} = \hat{M}_\eta \ddot{\eta}_d + \hat{C}_\eta \dot{\eta}_d + \hat{D}_\eta \dot{\eta}_d + \hat{g}_\eta(\eta) - K_p e(t) - K_d \dot{e}(t) \quad (41)$$

where $\eta_d = [x_d(t), y_d(t), z_d(t), \phi_d(t), \theta_d(t), \psi_d(t)]^T$ is the desired trajectory vector, $\dot{\eta}_d$ and $\ddot{\eta}_d$ are the first and second time derivatives of η_d , respectively. Also, the trajectory tracking error is expressed by $e(t) = [e_1(t), \dots, e_6(t)]^T = \eta - \eta_d$ and $\dot{e}(t)$ is its time derivative. The PD controller feedback gains are defined by $K_p, K_d \in \mathbb{R}^{6 \times 6}$, diagonal positive definite matrices.

Based on the real-time experiments reported in Campos et al. (2017), the PD controller performs well when the robot is working under nominal controlled conditions. However, when some parameters such as the buoyancy or the damping change, the controller performance is severely degraded, and the robot cannot follow properly the reference trajectories. To overcome this issue, we propose to enhance the PD controller by injecting the external disturbance estimation generated by the proposed disturbance observer to be compensated. Moreover, it is worth to note that the proposed observer has two gains tuned automatically according to the adaptation dynamics in (16).

Finally, the proposed control law for the enhanced PD controller (ePD) is given as follows:

$$\tau_\eta(\eta) = \tau_{nom} - \hat{M}(\cdot)\hat{d} - \hat{K} \text{SGN}(\dot{e}) \quad (42)$$

where τ_{nom} is the control law given in (41), $\hat{d}(t)$ is the disturbance estimation generated by the observer dynamics (11). The vector $\text{SGN}(\dot{e})$ is defined as $\text{SGN}(\dot{e}) = [\text{sgn}(\dot{e}_1(t)), \dots, \text{sgn}(\dot{e}_6(t))]$ and \hat{K} is an adaptive gain, computed from the following dynamic equation:

$$\dot{\hat{K}} = \beta \|\dot{e}\| \quad (43)$$

where $\beta \in \mathbb{R}$ is a real positive constant.

It is worth to note, from the proposed control law (42), that the second term \hat{d} is the observer's external disturbance/parametric uncertainties vector estimation. Besides, the third term is added to give more robustness to the proposed controller. However, this term could generate a chattering effect in the control input and should carefully tuned to avoid such an effect.

Finally, the closed-loop dynamics stability analysis is given in the sequel.

5.1. Closed-loop stability analysis

First, consider the dynamic model of the underwater vehicle (4), then by introducing the control law (42), we obtain the following closed-loop system:

$$\frac{d}{dt} \begin{bmatrix} e \\ \dot{e} \end{bmatrix} = \begin{bmatrix} \dot{e} \\ -M_\eta(\eta)^{-1} \left[[\hat{C}_\eta(v, \eta) + \hat{D}_\eta(v, \eta) + K_d] \dot{e} + K_p e \right. \\ \left. + \hat{K} \text{SGN}(\dot{e}) \right] - \hat{d}(t) + d(t) \end{bmatrix} \quad (44)$$

Second, consider the following Lyapunov candidate function:

$$V(e, \dot{e}) = \frac{1}{2} \dot{e}^T \hat{M}_\eta(\eta) \dot{e} + \int_0^e \xi^T K_p(\xi) d\xi + \frac{1}{2\beta} \tilde{K}^2 \quad (45)$$

where β is a positive constant introduced in (43), and the parameter estimation error is defined by $\tilde{K} = \hat{K} - K$. Additionally, the integral term is defined as follows:

$$\int_0^e \xi^T K_p(\xi) d\xi = \int_0^{e_1} \xi_1 k_{p_1}(\xi_1) d\xi_1 + \dots + \int_0^{e_6} \xi_6 k_{p_6}(\xi_6) d\xi_6$$

Then, consider the following inequality:

$$e_j k_{p_j} > \alpha_j (|e_j|) \quad \text{for } j = 1, \dots, 6$$

Which is satisfied by considering class-K functions $\alpha(\cdot)$ as reported in Campos et al. (2017). Consequently, we can conclude that:

$$\int_0^e \xi^T K_p(\xi) d\xi > 0, \quad \forall e \neq 0 \in \mathbb{R}^n \quad (46)$$

and

$$\int_0^e \xi^T K_p(\xi) d\xi \rightarrow \infty \quad \text{as } \|e\| \rightarrow \infty \quad (47)$$

From (46) and (47), one can ensure that the proposed Lyapunov function is positive definite and radially unbounded. Then, taking the time derivative of V leads to:

$$\dot{V}(e, \dot{e}) = \dot{e}^T \hat{M}_\eta(\eta) \ddot{e} + \frac{1}{2} \dot{e}^T \dot{\hat{M}}_\eta(\eta) \dot{e} + e^T K_p \dot{e} + \frac{1}{\beta} \tilde{K} \dot{\tilde{K}} \quad (48)$$

Now, injecting the error dynamics (44) into (48), yields:

$$\begin{aligned} \dot{V}(e, \dot{e}) &= \frac{1}{2} \dot{e}^T \left[\dot{\hat{M}}_\eta(\eta) - 2\hat{C}_\eta(v, \eta) \right] \dot{e} - \dot{e}^T \left[\hat{D}_\eta(v, \eta) + K_d \right] \dot{e} \\ &\quad + \dot{e}^T [d(t) - \hat{d}(t)] - \hat{K} \dot{e}^T \text{SGN}(\dot{e}) + \frac{1}{\beta} \tilde{K} \dot{\tilde{K}} \end{aligned} \quad (49)$$

Recalling an important property of the dynamic model, within the Lagrangian approach, that is $[\dot{\hat{M}}_\eta(\eta) - 2\hat{C}_\eta(v, \eta)]$ is a skew-symmetric matrix, Fossen (1999). Then, \dot{V} can be simplified as:

$$\dot{V}(e, \dot{e}) = -\dot{e}^T \left[\hat{D}_\eta(v, \eta) + K_d \right] \dot{e} + \dot{e}^T [d(t) - \hat{d}(t)]$$

$$\begin{aligned} & - \hat{K} \dot{e}^T \text{SGN}(\dot{e}) + \frac{1}{\beta} \tilde{K} \dot{\tilde{K}} \\ &= -\dot{e}^T \left[\hat{D}_\eta(v, \eta) + K_d \right] \dot{e} + \dot{e}^T [d(t) - \hat{d}(t)] \\ & - \hat{K} \sum_{i=0}^6 |\dot{e}_i| + \frac{1}{\beta} \tilde{K} \dot{\tilde{K}} \\ &\leq -\lambda_{\min} \{ \hat{D}_\eta(v, \eta) + K_d \} \|\dot{e}\|^2 + K \|\dot{e}\| \\ & - \hat{K} \|\dot{e}\| + \tilde{K} \|\dot{e}\| \\ &= -\lambda_{\min} \{ \hat{D}_\eta(v, \eta) + K_d \} \|\dot{e}\|^2 \end{aligned} \quad (50)$$

In (50), the matrix K_d was selected as positive definite in the control design, and the damping matrix is $\hat{D}_\eta > 0$ (see Fossen (1999)). This means that the function \dot{V} is negative semi-definite. However, we can conclude that the equilibrium point is asymptotically stable by applying Krasovskii-Lasalle's invariance principle (Khalil (2015)).

6. Real-time experimental results

The proposed approach was experimentally tested in different operating conditions to demonstrate its effectiveness and robustness. It was tested on the "Leonard" Unmanned Underwater Vehicle (UUV), developed at LIRMM laboratory, located at the University of Montpellier in France. The robot is a tethered vehicle with dimensions of 75 x 55 x 45 cm and a weight of 28 kg. It has six propellers, making it a fully actuated holonomic vehicle.

This UUV is controlled with a laptop computer featuring an Intel Core i7-3520M 2.9 GHz CPU and 8 GB memory. The proposed control scheme was programmed using Visual C++ language, and the laptop collects data from the robot's pressure and IMU sensors. The laptop then processes the data using the control algorithms and transmits the commands to the six Syren10 Motor Drives that regulate the robot's actuators. Table 1 provides an overview of the primary features of Leonard underwater vehicle.

To demonstrate the effectiveness and robustness of the proposed control solution, several experimental tests were conducted in the engineering pool of LIRMM. The test pool has dimensions of 4 Å 3 Å 2 m and a capacity of approximately 24 000 liters. Without loss of generality, the conducted experiments are mainly focused on depth and yaw dynamics, even though the control laws developed were intended for the whole six-degree-of-freedom system. The main objective of the control law is to accurately track a pre-defined trajectory for depth and yaw in presence of external disturbances and parametric uncertainties. The developed controllers were then implemented on the Leonard underwater vehicle for the experimental investigations considered in this paper.

6.1. Performance evaluation criteria

To ensure a fair comparison of the performance of each controller in tracking the reference trajectory, we propose to use the following criteria:

Table 1
Main Features of the underwater vehicle

Mass	28 kg
Buoyancy	9 N
Dimensions	75 × 55 × 45 cm
Maximal depth	100m
Thrusters	6 Seabotix BTD150
Power	24V - 600 W
Attitude Sensor	Invensense MPU-6000 MEMS 3-axis gyro and accelerometer 3-axis I2C magnetometer HMC-5883L Atmega328 microprocessor
Camera	Pacific Co. VPC-895A CCD1/3 PAL-25-fps
Depth sensor	Pressure Sensor MS5803-02BA
Sampling period	50 ms
Surface computer	Dell Latitude E6230- Intel Core i7 -2.9 GHz Windows 10 Professional 64 bits Microsoft Visual C++ 2015
Tether length	30 m

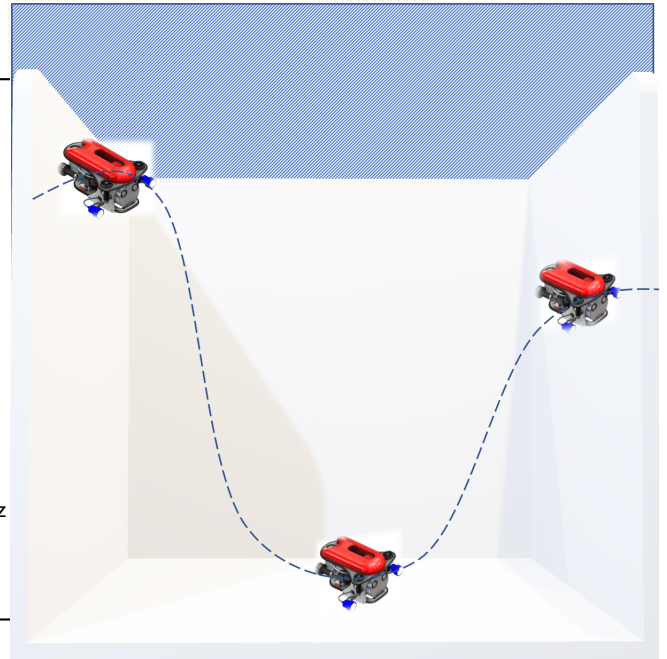


Figure 2: Setup for the nominal case. The robot tracks a desired trajectory in depth (dashed line) and yaw simultaneously without considering parametric uncertainties or external disturbances.

- Root Mean Square Error (RMSE) - This metric is defined as:

$$RMSE = \sqrt{\frac{1}{T_f} \int_0^{T_f} \|e(t)\|^2 dt} \quad (51)$$

where T_f is the duration of the experimental test, and $e(t)$ is the tracking error.

- In order to assess the amount of energy used, we suggest utilizing the integral of the control input index, denoted as INT. This metric is calculated as the integral of the absolute values of the position/attitude control input vector, denoted by $\tau(t)$, throughout the experiment duration, from t_i (the initial time) to t_f (the final time), as expressed in the following equation:

$$INT = \int_{t_i}^{t_f} |\tau(t)| dt \quad (52)$$

Using this criteria, we can accurately evaluate the energy consumed during the experiment.

6.2. Real-Time experimental scenarios

Several real-time experiments were conducted to validate the effectiveness and robustness of the proposed control scheme, including:

1. *Nominal scenario:* This test was conducted without external disturbances, where the robot should track a reference trajectory in depth and yaw simultaneously (see illustration of Figure 2).
2. *Robustness towards parametric uncertainties:* The hydrodynamic parameters of the underwater vehicle are modified to test the proposed controller's robustness.

A floater was attached to the vehicle's body to modify its buoyancy, and a rigid plastic sheet, measuring 45 cm × 20 cm, was attached to the body of the vehicle to change its damping. Both the floater and plastic sheet can be seen in Figure 3.

3. *Robustness towards sudden mass variation:* In this scenario, the robot should carry a payload for a while and then release it. To demonstrate this situation, a 60-cm long rope holding a 335-gram mass was attached to the robot's body, as illustrated in Figure 4.
4. *Robustness towards external disturbances:* In this scenario, external disturbances were applied to the robot while tracking the reference trajectory. A stick was used to push the robot several times, as illustrated in Figure 5.

For all these scenarios, the underwater vehicle should track a reference trajectory in depth and yaw simultaneously, as shown in Figure 6.

6.3. Scenario 1: Nominal Scenario

The results of the trajectory tracking for depth and yaw dynamics are shown in the top part of Figure 7, respectively. The trajectory tracking for depth dynamics is shown on the left part. As we can see, the proposed controller has better tracking error than the nominal PD because this last one has a steady state tracking error. Besides, when we analyze the yaw trajectory tracking performance, we notice that both controllers perform well. The tracking errors for both degrees of freedom are plotted in the middle part of Figure 7. Finally, in the lower part of Figure 7, the evolution of the

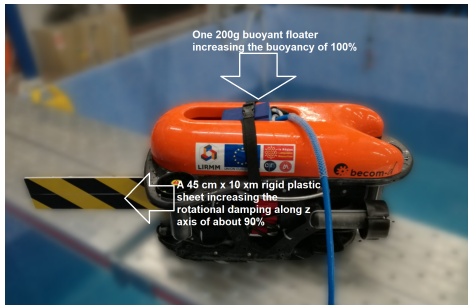


Figure 3: Setup configuration for scenario 2. We fixed a rigid plastic sheet to modify the damping of the vehicle. Also, we attached a floater to increase the vehicle's floatability.

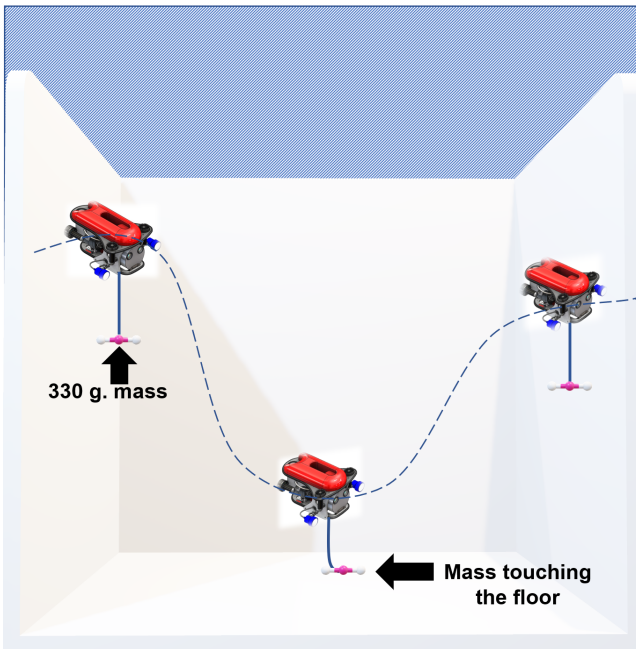


Figure 4: Setup configuration for scenario 3. In this scenario, we attach a weight to the vehicle's body to suddenly modify the mass carried by the vehicle when the depth changes.

control inputs versus time is shown. We can observe that both controllers have a similar energy consumption behavior.

In Figure 8, the evolution of the adaptive feedback observer gains is shown. From this figure, one can notice that the gains grow linearly until the real sliding mode condition is reached. The gains for the depth controller are shown in the left part, and those for the yaw dynamics are depicted in the right part.

To quantify and fairly compare the PD and the proposed ePD, the RMSE is computed as summarized in the first row of Table 2. This table shows that the proposed controller has better tracking errors compared to the original PD controller. However, for the yaw tracking, the PD control performs better, showing a smaller RMSE. The energy consumption for both controllers is summarized in the first row of Table 3. As expected, the proposed ePD demands slightly more energy than the original PD.

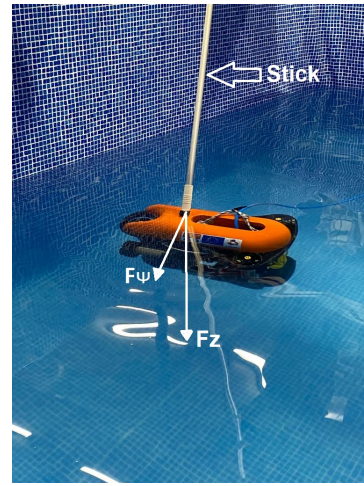


Figure 5: Setup configuration for scenario 4. Using a stick, we apply aggressive external disturbances to the vehicle's body.

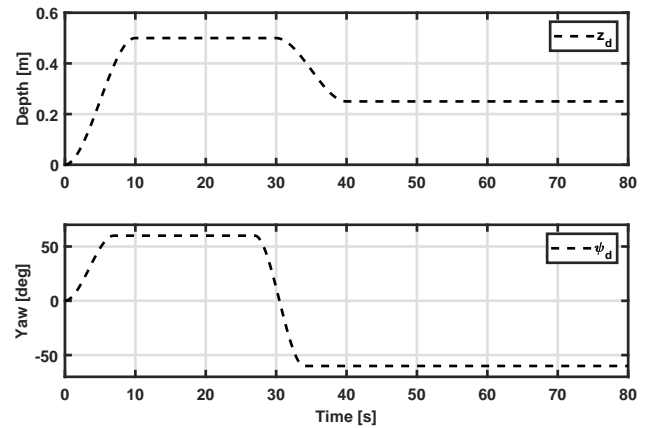


Figure 6: Desired depth and yaw trajectories used in all the proposed scenarios.

Finally, the main objective behind the proposed observer was to estimate both external disturbances and parametric uncertainties. The estimation generated by the proposed observer can be seen in the first row of Figure 15.

6.4. Scenario 2: Robustness to parametric uncertainties

In this scenario, we have modified the hydrodynamic parameters of the robot as explained in Section 6.2. As we can see in Figure 3, we have attached a single floater to increase the floatability of the vehicle up to 100%, to introduce parametric uncertainties in the depth dynamics. Furthermore, we have fixed a rigid plastic sheet of dimensions $45\text{ cm} \times 10\text{ cm}$ to increase the damping of the vehicle up to 90% affecting the yaw dynamics.

The trajectory tracking for depth and yaw dynamics in this scenario are shown at the top part of Figure 9. For the depth dynamics, we can observe from the PD performance (solid blue line), that the controller fails to track the desired trajectory because it shows a steady-state tracking error

during this test. In contrast, for the proposed scheme based on the disturbance observer, we can notice that the controller performs well with a tracking error around the origin. The trajectory tracking for the yaw dynamics is shown in the left part of the figure. Both controllers perform well until the last 20 seconds of the test, where we can observe an increase in the tracking error of the original PD controller. In the middle of Figure 9, the tracking errors for this experiment are plotted. Finally, in the bottom part of the figure, we show the evolution versus time of the control inputs. Note that the chattering effect is not present for this test.

In Figure 10, we can observe the evolution of the controller feedback gains. These gains increase linearly during the first seconds of the test, then they remain at a constant value when the sliding surface is reached.

The values of the RMSE metric are given in the second row of Table 2; analyzing the obtained values, we can conclude that the proposed ePD outperforms the PD controller.

Regarding energy consumption, both controllers behave apparently in the same way, as stated in the second row of Table 3.

The observed disturbance given by the estimator is shown in the second row of Figure 15.

6.5. Scenario 3: Robustness to mass variation

In this scenario, we try to reproduce a situation where the robot is autonomously carrying an object and will release it for a certain time. In particular, we have attached a 330-g weight to the vehicle’s body. The added extra mass will change the robot’s initial position, so when the experiment starts, the robot subject to the added payload will track the desired trajectory. Then, when the robot moves down to 50 cm in depth, the weight will touch the floor, suddenly changing the mass of the vehicle and affecting its dynamics.

The results of this experiment are shown in Figure 11. The trajectory tracking for depth reference is shown in the left part of the figure. We can observe that, for the depth, the proposed ePD controller has slightly more oscillations than the original PD controller. Also, both controllers perform well in the trajectory tracking of the desired yaw dynamics. In the middle part of the figure, the resulting tracking errors are plotted. Finally, at the bottom part of the figure, we can notice the oscillatory behavior in the generated control input of the depth. These oscillations are due to the constant increase of the controller feedback gains, as shown in Figure 12, where we can observe that the gains are growing during the experiment. Solving this challenging issue is a part of our future work.

Finally, the values of RMSE metric for this experiment are given in the third row of Table 2. The INT metric is shown in the third row of Table 3.

The observed disturbance for this experiment generated by the proposed estimator is plotted in the third row of Figure 15.

6.6. Scenario 4: External disturbance rejection

The last test is about the robustness of the proposed controller towards aggressive external disturbances. As illustrated in Figure 5, we apply disturbances by hand to the robot using a long stick trying to affect the depth and yaw dynamics during the trajectory tracking.

The obtained results of this scenario are shown in Figure 13. In the top part of the figure, we plotted the trajectory tracking for both dynamics. We can observe that we disturbed the depth dynamics six times and the yaw three times. From this figure, we can see a fast recovery of the vehicle when it is externally disturbed. The resulting tracking errors for both dynamics are plotted in the middle part of the figure. Finally, at the bottom part, the evolution of the input signals is shown. As expected, the controller tries to counteract and to compensate for external disturbances.

The values of RMSE metric for this experiment are given in the third row of Table 2. The INT metric is shown in the third row of Table 3.

The observed disturbance for this experiment generated by the proposed estimator is plotted in the third row of Figure 15.

Finally, note that we cannot compare our proposed scheme with the original PD controller for this experiment since it is impossible to reproduce precisely and exactly the same disturbances for both controllers.

Table 2
RMSE comparison criteria for PD and ePD

Case	PD		ePD	
	Depth (m)	Yaw (deg)	Depth (m)	Yaw (deg)
1	0.0151	0.1418	0.0037	0.2955
2	0.0613	2.1718	0.0069	0.0644
3	0.0069	1.0053	0.0053	0.0142
4	–	–	0.0006	0.3421

Table 3
Energy consumption comparison criteria through the INT indicator for PD and ePD

Case	PD		ePD	
	Depth	Yaw	Depth	Yaw
1	3221	414	3487	308
2	7634	731	7049	462
3	1902	509	2363	541
4	–	–	3525	533

7. Conclusions

In this paper, we have designed an enhanced robust PD controller to resolve the problem of trajectory tracking in underwater robotics. This controller mixes the nominal PD control law with an adaptive disturbance observer based on the Super-Twisting algorithm. Roughly speaking, the

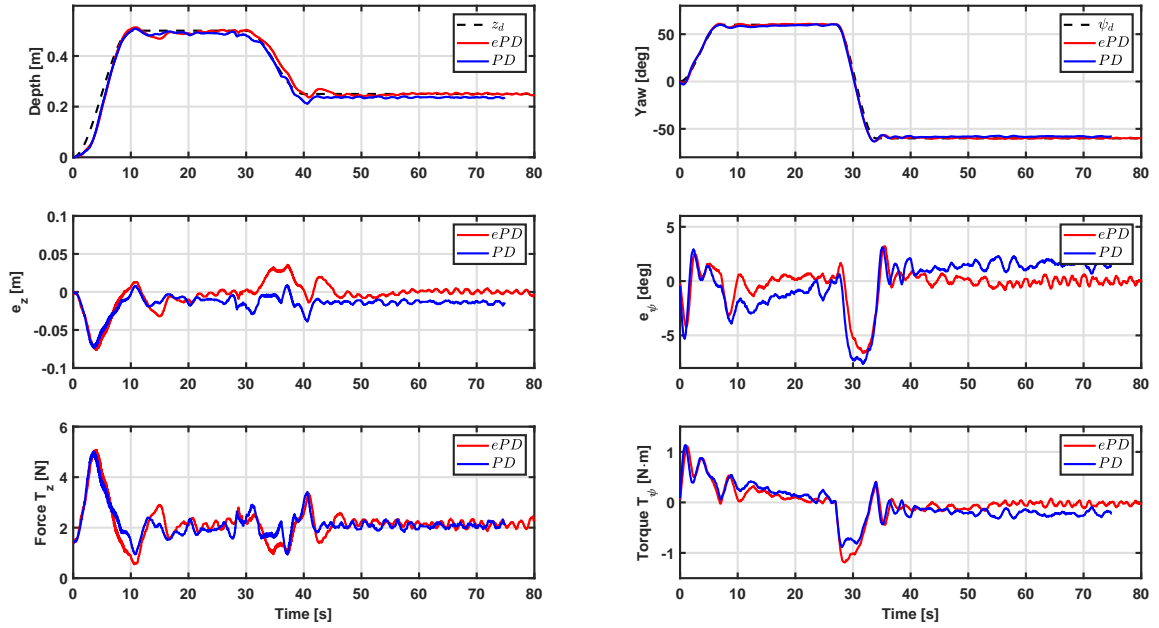


Figure 7: Scenario 1 - Nominal Case. Experimental results of the trajectory tracking in depth and yaw, the desired trajectory is represented by the black dashed line, the PD with a blue solid line, and the proposed ePD controller with a red solid line.

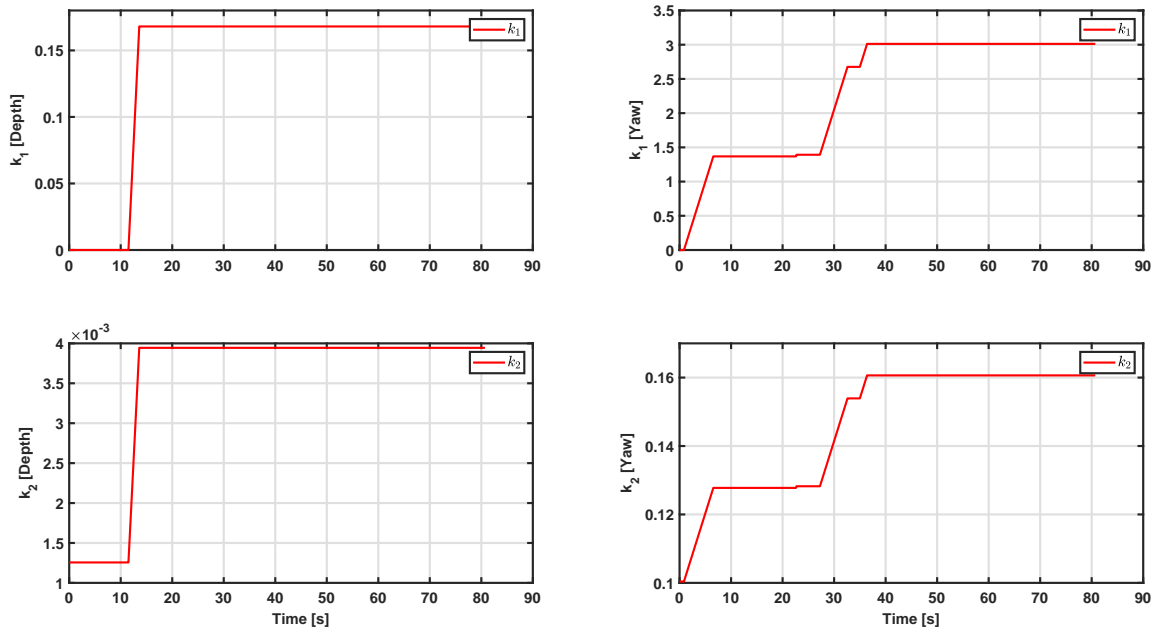


Figure 8: Scenario 1 - Nominal Case. Evolution of the adaptive gains of the controller in depth (left) and yaw (right) dynamics.

observer online estimates the external disturbances and parametric uncertainties, allowing the controller to compensate for them. Lyapunov arguments provide the stability of the resulting closed-loop controller/observer architecture. Finally, several real-time experiments were conducted, in different

operating conditions, to demonstrate the proposed scheme's effectiveness and robustness. The proposed controller is compared with the nominal PD design and shows better performance in all these experiments.

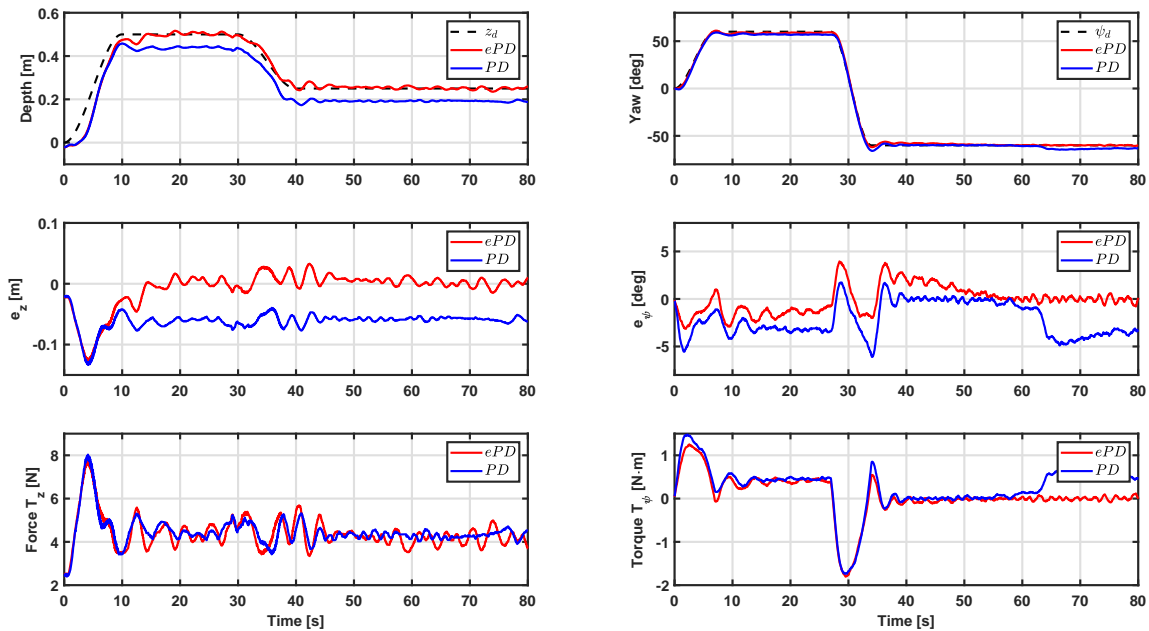


Figure 9: Scenario 2 - Robustness towards parametric uncertainties. Experimental results of the trajectory tracking in depth and yaw, the desired trajectory is represented by the black dashed line, the PD with a blue solid line, and the proposed RPD controller with a red solid line.

Acknowledgements

This work was supported by the French Occitanie Region within the framework of the project "Défi-clé Robotique Centrée sur l'Humain" under Grant N° 21034741.

CRedit authorship contribution statement

Jesús Guerrero: Conceptualization of this study, Methodology, Software, Data collection, Original draft preparation. **Ahmed Chemori:** Software, Writing, Data Collection - Original draft preparation. **Vincent Creuze:** Software, Writing - Original draft preparation. **Jorge Torres:** Writing, Original and final draft preparation.

References

Campos, E., Chemori, A., Creuze, V., Torres, J., Lozano, R., 2017. Saturation based nonlinear depth and yaw control of underwater vehicles with stability analysis and real-time experiments. *Mechatronics* 45, 49–59.

Cui, R., Chen, L., Yang, C., Chen, M., 2017. Extended state observer-based integral sliding mode control for an underwater robot with unknown disturbances and uncertain nonlinearities. *IEEE Transactions on Industrial Electronics* 64, 6785–6795.

Fernandes, D.d.A., Sørensen, A.J., Pettersen, K.Y., Donha, D.C., 2015. Output feedback motion control system for observation class rovs based on a high-gain state observer: Theoretical and experimental results. *Control Engineering Practice* 39, 90–102.

Fossen, T.I., 1999. *Guidance and control of ocean vehicles*. University of Trondheim, Norway, Printed by John Wiley & Sons, Chichester, England, ISBN: 0 471 94113 1, Doctors Thesis .

Fossen, T.I., 2011. *Handbook of marine craft hydrodynamics and motion control*. John Wiley & Sons.

García-Valdovinos, L.G., Salgado-Jiménez, T., Bandala-Sánchez, M., Nava-Balazar, L., Hernández-Alvarado, R., Cruz-Ledesma, J.A., 2014. Modelling, design and robust control of a remotely operated underwater vehicle. *International Journal of Advanced Robotic Systems* 11, 1.

Guerrero, J., Torres, J., Antonio, E., Campos, E., 2018. Autonomous underwater vehicle robust path tracking: Generalized super-twisting algorithm and block backstepping controllers. *Control Engineering and Applied Informatics* 20, 51–63.

Guerrero, J., Torres, J., Creuze, V., Chemori, A., 2019a. Observation-based nonlinear proportional-derivative control for robust trajectory tracking for autonomous underwater vehicles. *IEEE Journal of Oceanic Engineering* .

Guerrero, J., Torres, J., Creuze, V., Chemori, A., Campos, E., 2019b. Saturation based nonlinear pid control for underwater vehicles: Design, stability analysis and experiments. *Mechatronics* 61, 96–105.

Guo, Q., Zhang, Y., Celler, B.G., Su, S.W., 2016. Backstepping control of electro-hydraulic system based on extended-state-observer with plant dynamics largely unknown. *IEEE Transactions on industrial Electronics* 63, 6909–6920.

Hall, C.E., Shtessel, Y.B., 2006. Sliding mode disturbance observer-based control for a reusable launch vehicle. *Journal of guidance, control, and dynamics* 29, 1315–1328.

Han, J., 1995. A class of extended state observers for uncertain systems. *Control and decision* 10, 85–88.

Han, J.Q., 1998. Auto disturbance rejection controller and it's applications. *Control and decision* 13, 19–23.

Ismail, Z.H., Putranti, V.W., 2015. Second order sliding mode control scheme for an autonomous underwater vehicle with dynamic region concept. *Mathematical Problems in Engineering* 2015.

Khalil, H.K., 2015. *Nonlinear control*. volume 406. Pearson New York.

Khodayari, M.H., Balochian, S., 2015. Modeling and control of autonomous underwater vehicle (auv) in heading and depth attitude via self-adaptive fuzzy pid controller. *Journal of Marine Science and Technology* 20, 559–578.

Levant, A., 1993. Sliding order and sliding accuracy in sliding mode control. *International Journal of Control* 58, 1247–1263. doi:10.1080/

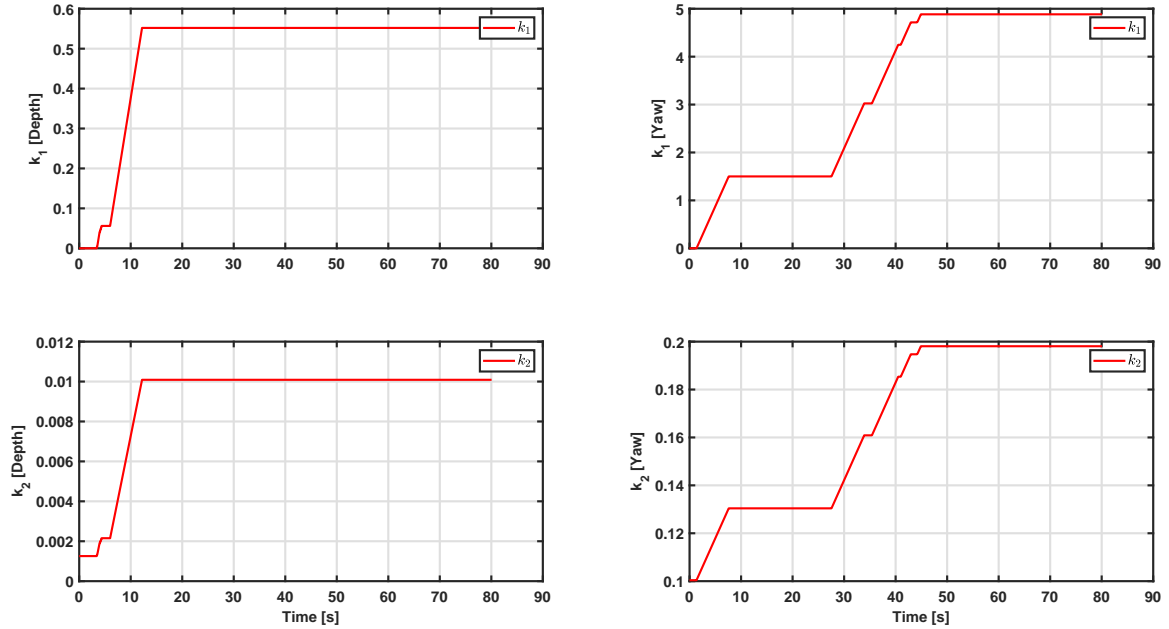


Figure 10: Scenario 2 - Robustness towards parametric uncertainties. Evolution of the adaptive gains of the controller in depth (left) and yaw (right) dynamics.

00207179308923053.

Li, J.H., Lee, P.M., 2005. Design of an adaptive nonlinear controller for depth control of an autonomous underwater vehicle. *Ocean engineering* 32, 2165–2181.

Li, Z., Wang, M., Ma, G., 2022. Adaptive optimal trajectory tracking control of auvs based on reinforcement learning. *ISA Transactions* doi:<https://doi.org/10.1016/j.isatra.2022.12.003>.

Sarhadi, P., Noei, A.R., Khosravi, A., 2016a. Model reference adaptive pid control with anti-windup compensator for an autonomous underwater vehicle. *Robotics and Autonomous Systems* 83, 87–93.

Sarhadi, P., Ranjbar, A., Khosravi, A., 2016b. Model reference adaptive pid control with anti-windup compensator for an autonomous underwater vehicle. *Robotics and Autonomous Systems* 83, 87–93. doi:[10.1016/j.robot.2016.05.016](https://doi.org/10.1016/j.robot.2016.05.016).

Sarhadi, P., Ranjbar, A., Khosravi, A., 2017. Model reference adaptive autopilot with anti-windup compensator for an autonomous underwater vehicle: Design and hardware in the loop implementation results. *Applied Ocean Research* 62, 27–36. doi:[10.1016/j.apor.2016.11.005](https://doi.org/10.1016/j.apor.2016.11.005).

Shen, C., Shi, Y., Buckham, B., 2018. Trajectory tracking control of an autonomous underwater vehicle using lyapunov-based model predictive control. *IEEE Transactions on Industrial Electronics* 65, 5796–5805. doi:[10.1109/TIE.2017.2779442](https://doi.org/10.1109/TIE.2017.2779442).

Tijjani, A.S., Chemori, A., Creuze, V., 2022. A survey on tracking control of unmanned underwater vehicles: Experiments-based approach. *Annual Reviews in Control* 54, 125–147. doi:<https://doi.org/10.1016/j.arcontrol.2022.07.001>.

Wadoo, S., Kachroo, P., 2017. *Autonomous underwater vehicles: modeling, control design and simulation*. CRC press.

Xiang, X., Yu, C., Lapierre, L., Z., J., Z., Q., 2015. Survey on fuzzy-logic-based guidance and control of marine surface vehicles and underwater vehicles. *Int. J. Fuzzy Syst* 20, 572–586. doi:[10.1007/s40815-017-0401-3](https://doi.org/10.1007/s40815-017-0401-3).

Yan, Z., Wang, M., Xu, J., 2019. Global adaptive neural network control of underactuated autonomous underwater vehicles with parametric modeling uncertainty. *Asian Journal of Control* 21, 1342–1354.

Zhang, L., Zhang, L., Liu, S., Zhou, J., Papavassiliou, C., 2018. Low-level control technology of micro autonomous underwater vehicle based on intelligent computing. *Cluster Computing*, 1–12.

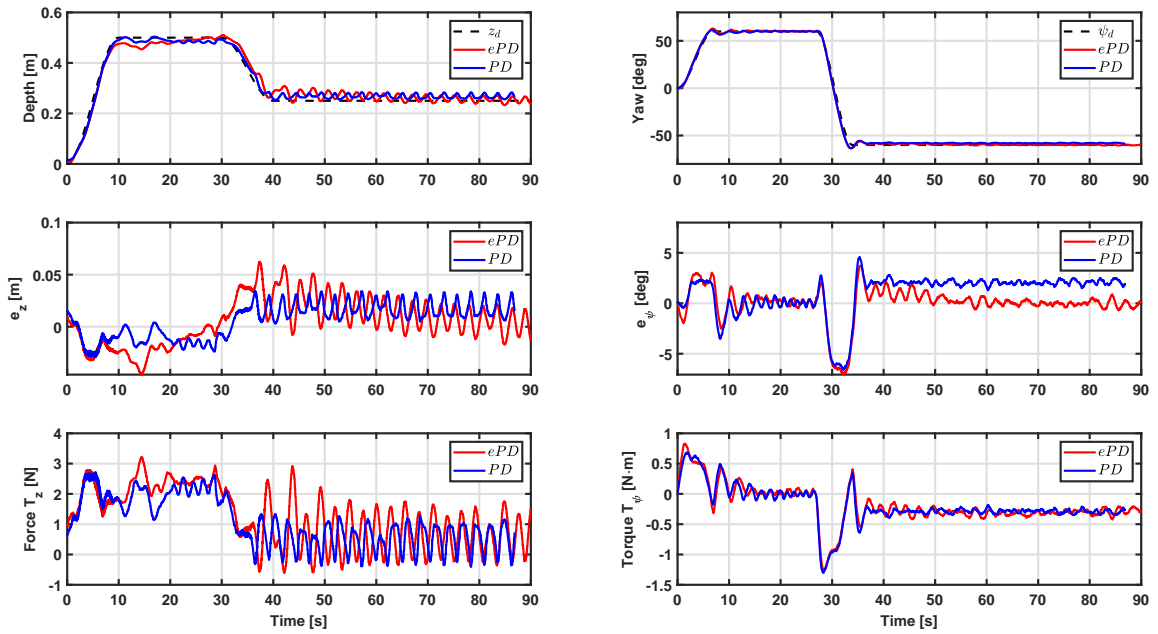


Figure 11: Scenario 3 - Robustness towards sudden mass change. Experimental results of the trajectory tracking in depth and yaw, the desired trajectory is represented by the black dashed line, the PD with a blue solid line, and the proposed ePD controller with a red solid line.

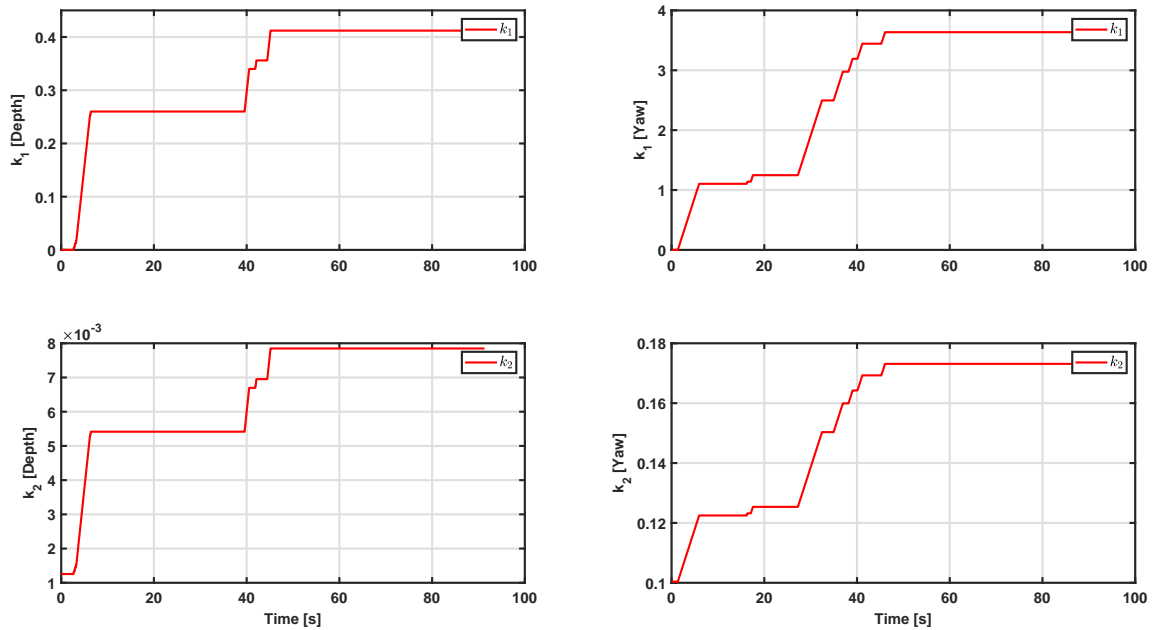


Figure 12: Scenario 3 - Robustness towards sudden mass change. Evolution of the adaptive gains of the controller in depth (left) and yaw (right) dynamics.

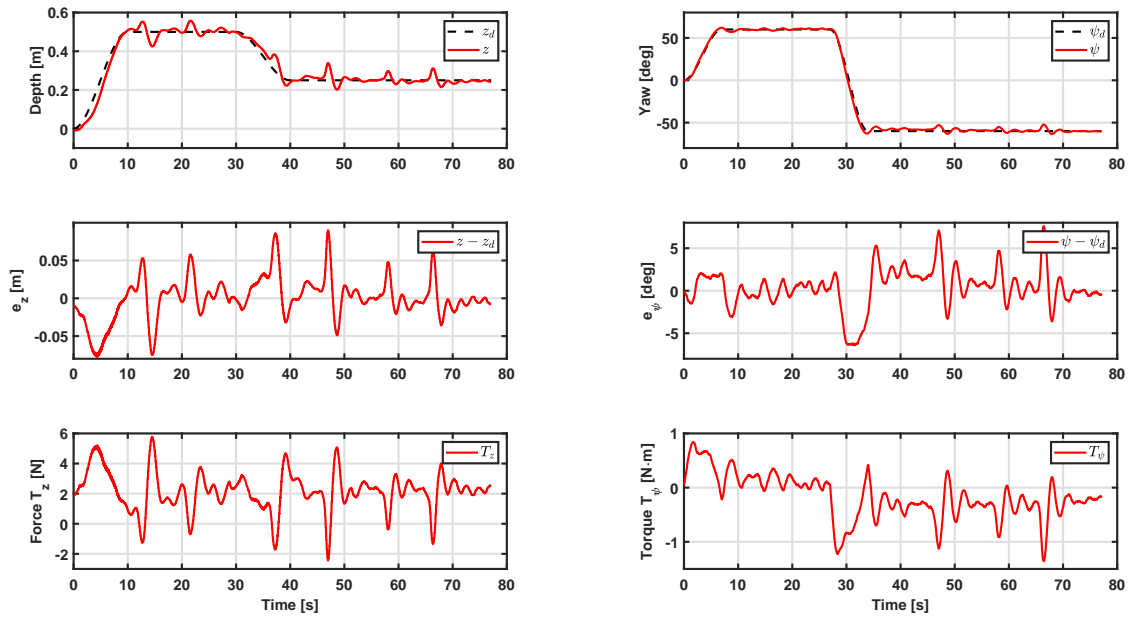


Figure 13: Scenario 4 - Robustness towards external disturbance rejection. Experimental results of the trajectory tracking in depth and yaw, the desired trajectory is represented by the black dashed line, the PD with a blue solid line, and the proposed ePD controller with a red solid line.

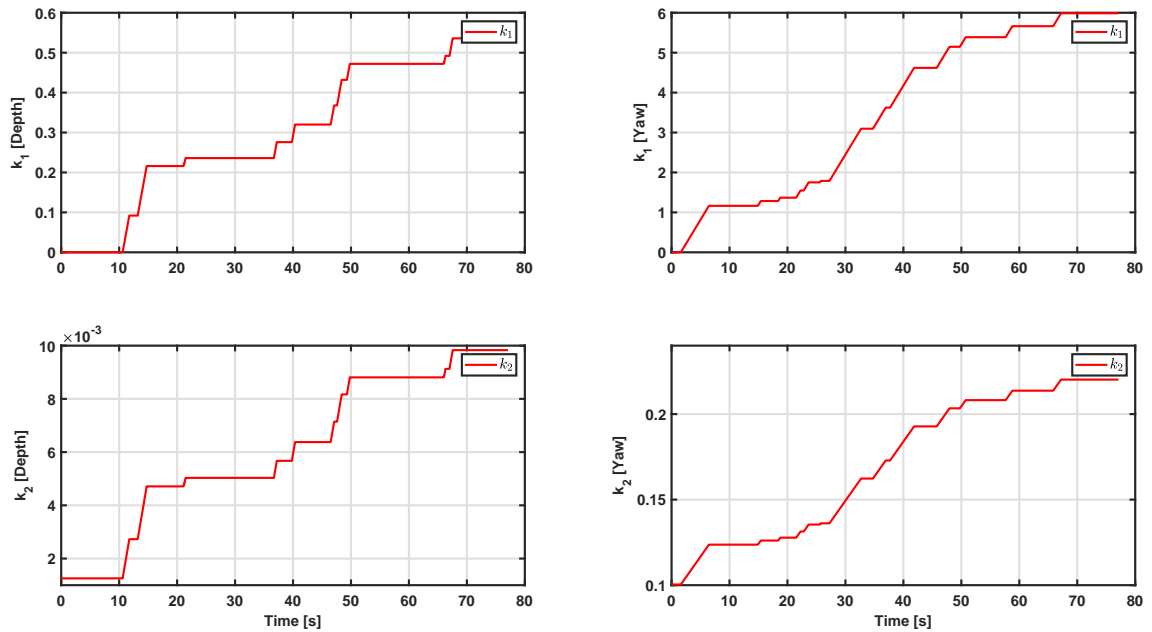


Figure 14: Scenario 4 - Robustness towards external disturbance rejection. Evolution of the adaptive feedback gains of the controller in depth (left) and yaw (right) dynamics.

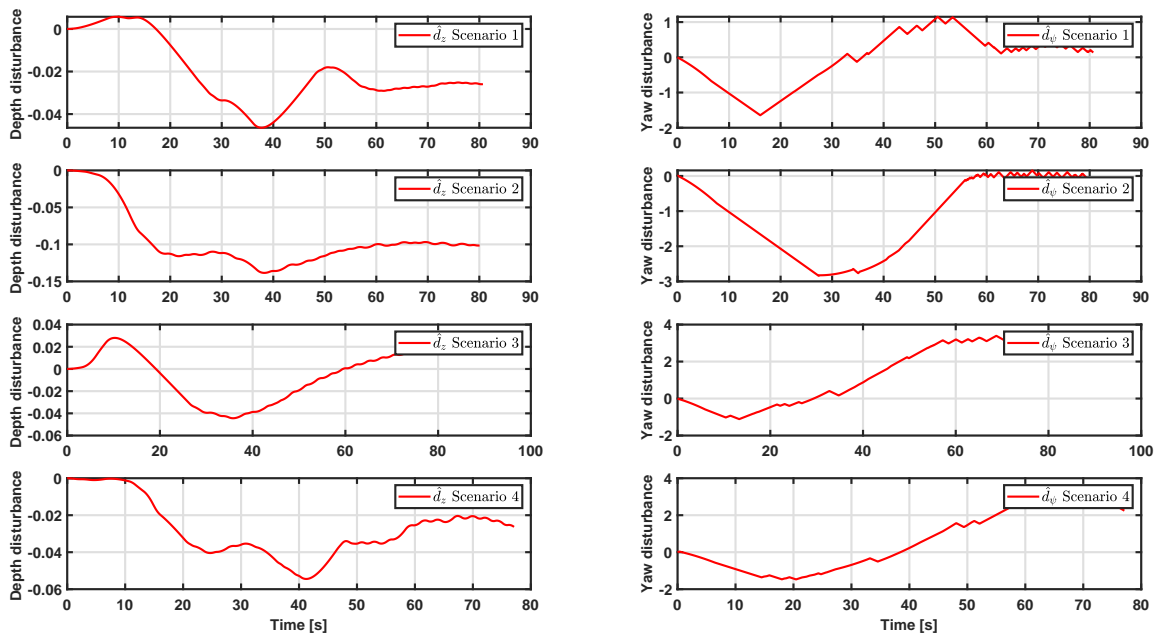


Figure 15: Estimation of the external disturbances generated by the proposed adaptive observer for the nominal (first row), parametric uncertainties (second row), sudden change of the mass (third row), and external disturbance rejection (fourth row) scenarios.